SIMULATION OF HIGH VOLTAGE TRANSMISSION RATIO BASED SINGLE-STAGE THREE-PHASE CURRENT-SOURCE PHOTOVOLTAIC GRID-CONNECTED INVERTER

[1]K.LAXMI PRASANNA, [2]K.PRAKASH CHARY

[1]M.tech, VAAGDEVI COLLEGE OF ENGINEERING, WARANGAL

[2]Assistant Professor VAAGDEVI COLLEGE OF ENGINEERING, WARANGAL

ABSTRACT--This paper presents a single stage three-phase current-source photovoltaic (PV) grid-connected inverter with high voltage transmission ratio (VTR) with Fuzzy Logic Control method. The control strategy, steady principle characteristics, and high-frequency switching process are analyzed profoundly, as well as the VTR's expression and design criterion of the center tapped energy storage inductor. Also, an improved zone sinusoidal pulse width modulation (SPWM) control strategy and an active-clamped sub circuit that can suppress the energy storage switch's turn-off voltage spike are introduced. The proposed control strategy consists of two control loops, namely, the outer loop of input dc voltage of PV cells with the maximum power point tracking fuzzy method and the inner loop of the energy storage inductor current. The simulation model has been implemented by using MATLAB and results are shown. Nonetheless, it has small energy storage inductor and output CL filter, low output current total harmonic distortion, and flexible voltage configuration of the PV cells. This study provides an effective design method for single-stage three-phase inverting with high VTR.

I INTRODUCTION

At present, the photovoltaic (PV) grid-connected power generation systems commonly adopt the voltage source circuit, which requires the value of dc voltage higher than the peak value of ac voltage. Therefore, an obvious defect arises. When the output capability of the PV cells weakens, i.e., in rainy day or at night, the operation of the whole system stops, along with the decrease of its utilization rate [1]–[6].

PV cells operate as current source, therefore, the current source inverter (CSI) is more suitable for the PV power generation system. Compared with the voltage-source inverter, the CSI has the following characteristics [7]–[17]:

1) Boosting feature, the input dc current can be manipulated by controlling the magnetizing time of the energy storage inductor, so as to realize the whole process of light utilization from weak to strong;

2) Direct control of the output current, thus it is more convenient and reliable to realize maximum power point tracking (MPPT), yet the

voltage source inverter can cause a dc bus crash and the reliability is accordingly reduced;

3) Inductor as the energy storage component, thus the system operation time is longer than that of the voltage source inverter, which uses the electrolytic capacitor as energy storage component;

4) Timely protection for overcurrent, which provides a high reliability.

The single-stage three-phase current-source PWM inverter with low voltage transmission ratio (VTR) proposed in [12]– [17] has the advantages of single-stage power conversion, boosting feature, and timely overcurrent protection, but there still exists the flaws. The VTR is not high enough, and the output waveform quality and conversion efficiency will be seriously affected when the input voltage is too low or the input voltage variation range is too wide

This would cause some problems such as poor dynamic characteristics, decrease of the VTR caused by the circuit parasitic parameters, large energy storage inductor current and circuit loss, low conversion efficiency, and worse output waveform. Therefore, it is difficult to invert for low voltage of the PV cells. In order to overcome the limitations of the traditional voltage source PWM inverter [1]–[6] and single-stage three-phase current-source PWM inverter with low VTR [12]–[17], this paper proposes a single-stage three-phase CSI with high VTR, as well as the circuit topology and an improved zone sinusoidal pulse width modulation (SPWM) control strategy with two control loops.

II CIRCUIT TOPOLOGY AND CONTROL STRATEGY

A. Control Strategy

The circuit topology of a single-stage three-phase current source PV grid-connected inverter with high VTR is shown in Fig. 1. The circuit topology is sequentially cascaded by the input filter capacitor C, the center-tapped energy storage inductor L, three-phase inverting bridge with six serial blocking diodes and an output CL filter. An energy storage switch S is connected between the center tap of L and the negative end of the PV cells, the left and right turn's

number of L are N1 and N2, respectively. Compared to CSI with low VTR, a center tap of the energy storage inductor and an energy storage switch are added to the proposed CSI. An active-clamped sub circuit connected in parallel at both ends of S shown in Fig. 1 is proposed, in order to suppress the turn-off voltage spike of S, which is caused by the leakage inductor of L1.
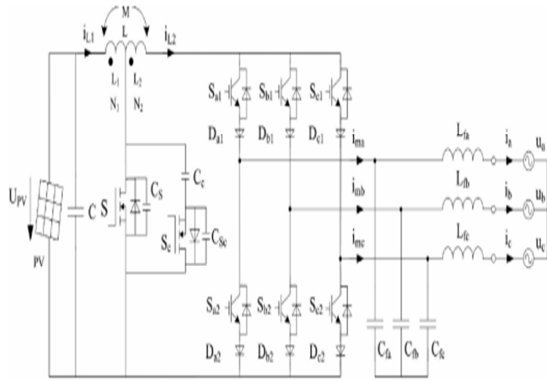

Fig. 1. Circuit topology of a single-stage three-phase current-source PV grid connected inverter with high VTR.

The VTR of the proposed CSI depends on both the energy storage duty ratio and the center tap position of L, and it provides a possibility to realize high VTR inverting.

B. Two-Loop Improved Zone SPWM Control Strategy

    1) **Improved Zone SPWM Control Strategy**: An improved zone SPWM control strategy is proposed in the single-stage three-phase current-source PV grid-connected inverter with high VTR. The reference signal that has the same frequency but different in phase of θ with the grid voltage is divided into six 60° intervals in a line cycle by the zero crossing point, thus there exist only two line voltages that is always $\geq \sqrt{6}/2Up$ in every 60° interval, where Up is root mean square (RMS) value of the phase voltage.

    This control strategy can ensure the normal operation of the CSI in any high-frequency (HF) switching period with the condition that output line voltage are not smaller than input voltage, i.e., $\sqrt{6}/2$ Up $\geq$ UPV , and obtain high quality of the output grid-connected current. Set the three-phase grid voltage ua, ub, and uc as

$$\begin{cases} u_a = \sqrt{2}U_p \sin(\omega t + \theta) \\ u_b = \sqrt{2}U_p \sin(\omega t - \frac{2\pi}{3} + \theta) \\ u_c = \sqrt{2}U_p \sin(\omega t - \frac{4\pi}{3} + \theta) \end{cases} \quad (1)$$

Three-phase reference signals ea, eb, and ec, which have the same frequency but phase difference

of θ with the grid voltages u_a, u_b, and u_c are, respectively, given by

$$\begin{cases} e_a = \sin(\omega t) \\ e_b = \sin(\omega t - \frac{2\pi}{3}) \\ e_c = \sin(\omega t - \frac{4\pi}{3}) \end{cases} \quad (2)$$

The aforementioned equation can also be expressed as Fig. 2(c). The improved zone SPWM control strategy needs to judge the intervals in a line cycle first. The control signals of power switches in different intervals should match Table I in order to ensure the normal operation condition of the CSI in any HF switching period. From Table I, it can be seen that the operating modes of the inverter are also different in different 60° intervals. Taking the Interval I as an example, Sb2 is ON, Sa2, Sb1, and Sc2 are OFF, and the power switches S, Sa1, and Sc1 are SPWM modulated, as shown in Fig. 2(a). In Fig. 2(a), k is the sampling coefficient of the energy storage inductor current iL, and ILavg is the average value of iL in one HF switching period TS , TS/2 is the sawtooth carrier wave period.

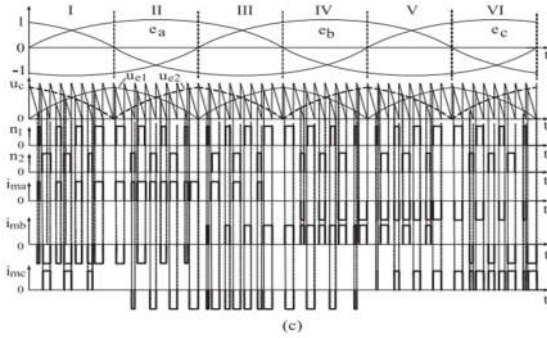**2) Two-Loop Improved Zone SPWM Control Strategy:**

(a)

(b)
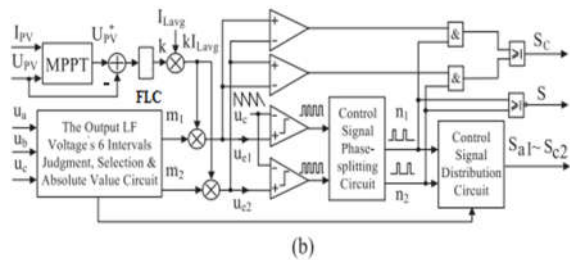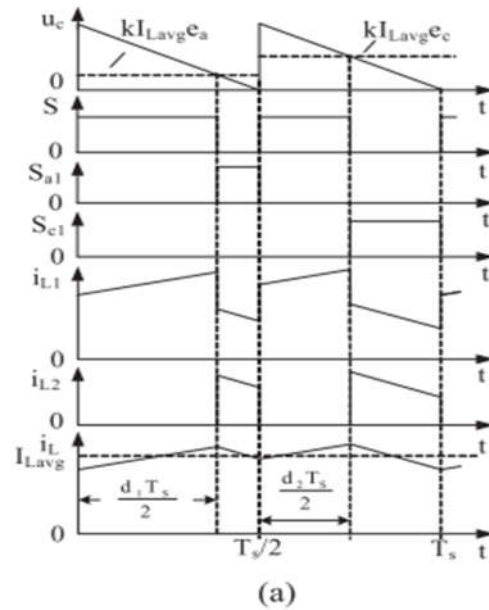
Fig. 2. Two-loop improved zone SPWM control strategy. (a) Generating of control signals in Interval I (b) Zone control diagram (c) Control principle waveforms.

Two loop improved zone SPWM control strategy of input dc voltage in outer loop and energy storage inductor current in inner loop is adopted in the proposed three-phase grid-connected inverter, as shown in Fig. 2(b) and (c). The grid-connected current reference signals ea, eb, and ec obtained by sampling the grid voltage ua, ub, and uc have phase difference θ with the grid voltage.

TABLE I
CONTROL SIGNALS OF THE POWER
SWITCHES IN DIFFERENT INTERVALS

Signal / Interval	m_1	m_2	S_{a1}	S_{a2}	S_{b1}	S_{b2}	S_{c1}	S_{c2}	S
I	e_a	e_c	n_1	0	0	1	n_2	0	
II	$-e_b$	$-e_c$	1	0	0	n_2	0	n_2	
III	e_b	e_a	n_1	0	n_2	0	0	1	n_1+n_2
IV	$-e_c$	$-e_a$	0	n_2	1	0	0	n_1	
V	e_c	e_b	0	1	n_1	0	n_2	0	
VI	$-e_a$	$-e_b$	0	n_1	0	n_2	1	0	

Signals n1 and n2 of the power switches are obtained after the signal phase-splitting circuit because the frequency of the energy release switches is half the frequency of the carrier wave, and then, the signals of the energy storage switch S and the energy release switches of the three-phase inverting bridge are obtained by the signal distribution circuit according to Table I.

III STEADY PRINCIPLE
A. LF Mode Analysis

There are six operating intervals in a line cycle of the inverter, and each interval can be divided into three operating modes.
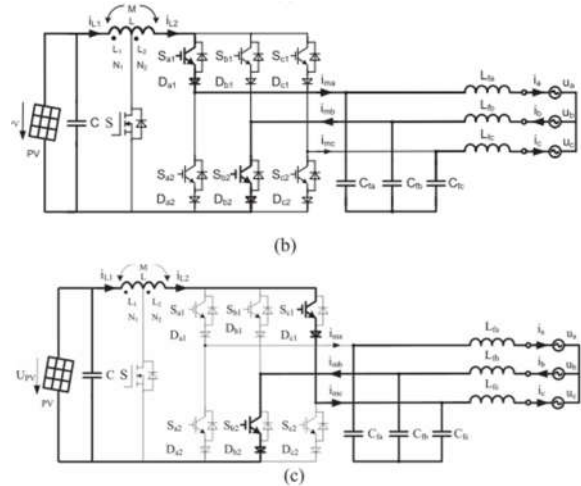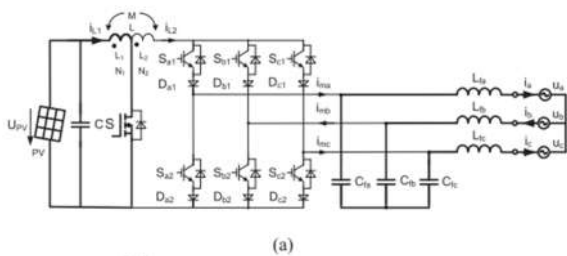

(a)

(b)

(c)

Fig. 3. Operating modes of the inverter in Interval I. (a) S ON, Sa1, Sc1 OFF, (b) Sa1 ON, S and Sc1 OFF, (c) Sc1 ON, S and Sa1 OFF.

Taking the Interval I in the Table I as an example, three operating modes of the inverter are shown in Fig. 3, when Sb2 is ON, Sa2, Sc2, and Sb1 are OFF.

**Mode I-1:** S is ON, Sa1 and Sc1 are OFF. Energy is stored to L1 and iL1 increases linearly with the rate of UPV/L1 via the path of UPV, L1, and S. ia, ib, and ic are maintained by Cf a, Cf b, and Cf c.

Mode I-2: Sa1 is ON, S and Sc1 are OFF. Since uab > UPV, i_L decreases linearly at the rate of (uab − UPV)/L via the path of UPV, L, and Sa1. UPV and L deliver energy to the grid **simultaneously. ic is maintained by Cf c.**

Mode I-3: Sc1 is ON, S and Sa1 are OFF. Since u_{cb} > U_{PV}, i_L decreases linearly with the rate of (u_{cb} − U_{PV})/L via the path of UPV, L, and Sc1, UPV and L deliver energy to the grid simultaneously. ia is maintained by Cf a.

B. VTR

1) Steady-State Solution of the State Variable: By neglecting the commutation overlap time of the power switches, the magnetizing and demagnetizing switching state equivalent circuits of the inverter are shown in Fig. 4, where the energy storage inductor current is in continuous conduction mode (CCM).
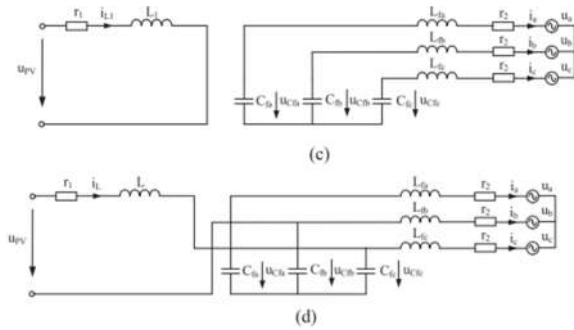

(a)

(b)

(c)

(d)
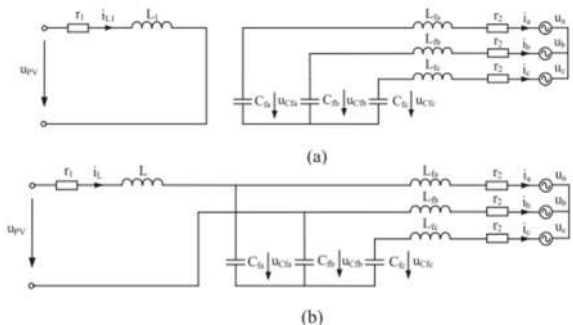
Fig. 4. Switching state equivalent circuits of the inverter in CCM mode. (a) 0∼d1 Ts /2 Magnetizing Period, (b) d1 TS /2∼Ts /2 Demagnetizing Period, (c) Ts /2∼(d2 + 1)Ts /2 Magnetizing Period, (d) (d2 + 1)Ts /2∼Ts Demagnetizing Period.

In steady state, the magnetizing and demagnetizing of the energy storage inductor basically reach balance, same as the charge and discharge of the capacitor within one TS, thus the state-space averaging method can be used to obtain the steady-state solution. By multiplying the state equations of Fig. 4(a) by d1/2 plus multiplying the state equations of the Fig. 4(b) by (1 − d1)/2 plus multiplying the state equations of Fig. 4(c) by d2/2 plus multiplying the state equations of Fig. 4(d) by (1 − d2)/2, with iL = iL1N1/(N1 + N2) substituted, the steady-state solution of the state variables is derived as equation (3) as shown at the bottom of the page.

2) VTR: Considering r2 = 0, following equation is derived from (3)

Set 1-d1=K$\sin wt = Ke_a$ (K∈(0,1)),so 1-d2=Ksin(wt-$\frac{4\pi}{3}$)=Ke$_c$,2-d1-d2=Ksin(wt-$\frac{2\pi}{3}$)=Ke$_b$.In interval I,$\left|\sin(wt - \frac{2\pi}{3})\right|$ can be expressed by the average value $\frac{3}{\pi}$, so d1+d2 ≈ 2-K,(4a) can be simplified

$$r_1\left[\frac{d_1}{2}\left(\frac{N_1+N_2}{N_1}\right)^2 + \frac{1-d_1}{2} + \frac{d_2}{2}\left(\frac{N_1+N_2}{N_1}\right)^2 + \frac{1-d_2}{2}\right]i_L = \left(1 + \frac{N_2}{N_1}\frac{d_1+d_2}{2}\right)U_{PV} - \frac{1-d_1}{2}u_a + \frac{2-d_1-d_2}{2}u_b - \frac{1-d_2}{2}u_c \quad (4a)$$

$$\frac{i_a}{i_c} = \frac{1-d_1}{1-d_2} = \frac{\sin(\omega t)}{\sin(\omega t - \frac{4\pi}{3})} \quad (4b)$$

$$\frac{i_a}{i_b} = \frac{1-d_1}{d_1+d_2-2} = \frac{\sin(\omega t)}{\sin(\omega t - \frac{2\pi}{3})} \quad (4c)$$

$$\frac{i_c}{i_b} = \frac{1-d_2}{d_1+d_2-2} = \frac{\sin(\omega t - \frac{4\pi}{3})}{\sin(\omega t - \frac{2\pi}{3})} \quad (4d)$$

$$\left(1 + \frac{N_2}{N_1}\frac{2 - 3K/\pi}{2}\right)U_{PV}$$

$$= K\left[u_a\sin(\omega t) + \frac{u_b}{2}\sin(\omega t - \frac{2\pi}{3}) + u_c\sin(\omega t - \frac{4\pi}{3})\right]$$

$$+ r_1\left[\frac{1}{2}\left(\left(\frac{N_1+N_2}{N_1}\right)^2\right)(2 - 3K/\pi) + 3K/2\pi\right]i_L \quad (5)$$

the input dc current IPV can be expressed as

$$I_{PV} = \frac{d_1 i_{L1}}{2} + \frac{1-d_1}{2}i_L + \frac{d_2 i_L}{2} + \frac{1-d_2}{2}i_L = \left[1 + \left(1 - 3K/2\pi\right)\frac{N_2}{N_1}\right]i_L \quad (6)$$

Assuming that the RMS of output phase current is I_P, the efficiency of the inverter is η, then

$$I_{PV} = 3U_P I_P/(U_{PV}\eta) \quad (7)$$

Derived from (6) and (7)

$$i_L = 3U_P I_P/\left\{U_{PV}\eta\left[1 + \left(1 - 3K/2\pi\right)\frac{N_2}{N_1}\right]\right\} \quad (8)$$

Substituting (1) and (8) into (4a), one can obtain

$$U_P = \frac{U_{PV}\left[1 + \frac{\left(\frac{N_2}{N_1}\right)(2 - 3K/\pi)}{2}\right]}{\frac{3\sqrt{2}K}{4} + 3I_P r_1\frac{\left[\frac{\left(\frac{N_1+N_2}{N_1}\right)^2(2 - 3K/\pi)}{2} + 3K/2\pi\right]}{U_{PV}\eta[1 + \left(\frac{N_2}{N_1}\right)(1 - 3K/2\pi)]}} \quad (9)$$

Assuming that r1 = 0, η = 100%, and the inverter in CCM mode, the ideal VTR Up/UPV is

$$\frac{U_P}{U_{PV}} = \frac{2\sqrt{2}\left[1 + \left(\frac{N_2}{N_1}\right)\right]}{3K} - \frac{\sqrt{2}\left(\frac{N_2}{N_1}\right)}{\pi} \quad (10)$$

Where the coefficient K is a constant for certain Up, U_{PV}, and N2/N1. To introduce the inner-loop feedback of the energy storage inductor current, set K = kILavg, thus the two-loop control strategy shown in Fig. 2 is obtained. Equation (10) can also be expressed as curves in Fig. 5. In Fig. 5: 1) for the same N2/N1, the larger energy storage duty ratio d1 and d2, the smaller energy release duty ratio 1 − d1, 1 − d2, the smaller coefficient K is, and the larger the VTR Up/UPV is; 2) for the same K, the larger

N2/N1, the larger Up/UPV is; and 3) when N2/N1 = 0, Up/Upv = 2√2/(3K) is the minimum, that is the VTR of the single-stage three phase current-source PV grid-connected inverter with low VTR. When UPV = 96 V, Up = 220 V, N2/N1 = 2, and K = 0.886. Therefore, the VTR of the proposed inverter can be adjusted by the duty ratio and the center-tapped turns ratio.
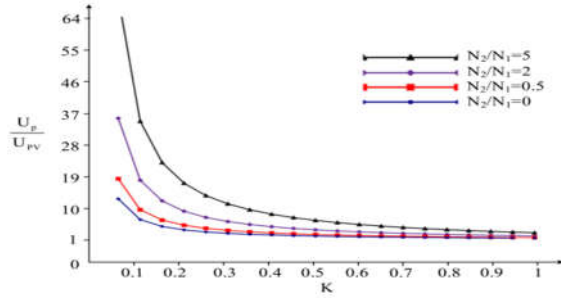

Fig. 5. Related curves between VTR of the proposed inverter with coefficient K.

C. **Steady State of Three-Phase Grid-Connected Current and the Reactive Power Regulated Angle θ**

Taking the Interval I as an example, two operating modes of the inverter within the former carrier wave period TS /2 are shown in Fig. 3(a) and (b). Set the initial value of i_L within the former carrier wave period TS /2 is $i_L(0)$, then the final value of iL is given by

$$i_L\left(\frac{T_S}{2}\right) = \left\{\left[i_L(0) + \frac{U_{PV}}{L_1}d_1\frac{T_S}{2}\right]\frac{N_1}{N_1+N_2} + \frac{U_{PV}-u_{ab}}{L}(1-d_1)\frac{T_S}{2}\right\}\frac{N_1+N_2}{N_1} = i_L(0) + \frac{U_{PV}}{L_1}d_1\frac{T_S}{2} + \frac{U_{PV}-u_{ab}}{L}(1-d_1)\times\frac{T_S}{2}\frac{N_1+N_2}{N_1} \quad (11)$$

Two operating modes of the inverter within the latter carrier wave period TS /2 are shown in Fig. 3(a) and (c). The final value of iL is given by

$$i_L(T_S) = \left\{\left[i_L\left(\frac{T_S}{2}\right) + \frac{U_{PV}}{L_1}d_2\frac{T_S}{2}\right]\frac{N_1}{N_1+N_2} + \frac{U_{PV}-u_{cb}}{L}(1-d_2)\frac{T_S}{2}\right\}\frac{N_1+N_2}{N_1} = i_L\left(\frac{T_S}{2}\right) + \frac{U_{PV}}{L_1}d_2\frac{T_S}{2} + \frac{U_{PV}-u_{cb}}{L}(1-d_2)\times\frac{T_S}{2}\frac{N_1+N_2}{N_1} \quad (12)$$

Within two carrier wave periods, the variation of iL is

$$\Delta i_L = i_L(T_S) - i_L(0) = \frac{U_{PV}}{L_1}d_1\frac{T_S}{2} + \frac{U_{PV}-u_{ab}}{L}(1-d_1)\times\frac{T_S}{2}\frac{N_1+N_2}{N_1} + \frac{U_{PV}}{L_1}d_2\frac{T_S}{2} + \frac{U_{PV}-u_{cb}}{L}(1-d_2)\frac{T_S}{2}\frac{N_1+N_2}{N_1} \quad (13)$$

Substituting (1) and (2) into the aforementioned equation and considering L/L1 =

[(N1 + N2)/N1]2, 1 − d1 = kILavgea, and 1 − d2 = kILavgec, the variation of iL is derived as

$$\Delta i_L = \frac{U_{PV}}{L_1}T_S - \frac{U_{PV}}{L_1}kI_{avg}|e_b|\frac{N_2}{N_1+N_2} - \frac{kI_{Lavg}}{L_1}\frac{3\sqrt{2}}{2}\frac{N_1}{N_1+N_2}\frac{T_S}{2}U_P\cos\theta \quad (14)$$

the magnetizing and demagnetizing of the energy storage inductor basically reach balance within one TS under steady state. Set ΔiL = 0, derived from the aforementioned equation

$$I_{Lavg} = \frac{2(N_1+N_2)U_{PV}}{N_2k|e_b|U_{PV}+(\frac{3\sqrt{2}}{2})N_1kU_P\cos\theta} \quad (15)$$

in Interval I, the average value of |eb| = |sin(ωt − 2π/3)| can be approximately expressed as 3/π, the aforementioned equation can be simplified as

$$I_{Lavg} = \frac{2(N_1+N_2)U_{PV}}{3N_2kU_{PV}/\pi+(\frac{3\sqrt{2}}{2})N_1kU_P\cos\theta} \quad (16)$$

It shows that ILavg is a constant in steady state. Within two carrier wave periods, the average value of the filtering capacitor current is approximate to zero, thus the average value of the Phase-a grid-connected current is approximately expressed as

$$i_{aavg} \approx I_{Lavg}\frac{N_1}{N_1+N_2}\frac{(1-d_1)\frac{T_S}{2}}{T_S} = \frac{N_1}{N_1+N_2}\frac{kI_{Lavg}^2}{2}e_a \quad (17)$$

Similarly, the average value of the Phase-c grid-connected current is approximately expressed as

$$i_{cavg} \approx I_{Lavg}\frac{N_1}{N_1+N_2}\frac{(1-d_2)\frac{T_S}{2}}{T_S} = \frac{N_1}{N_1+N_2}\frac{kI_{Lavg}^2}{2}e_c \quad (18)$$

Since $i_{aavg} + i_{bavg} + i_{cavg} = 0$, one could achieve

$$i_{bavg} \approx \frac{N_1}{N_1+N_2}\frac{kI_{Lavg}^2}{2}e_b \quad (19)$$

i_{aavg}, i_{bavg}, and i_{cavg} are separately changing with ea, eb , and ec in sinusoidal form, thus the symmetrical three-phase sinusoidal currents are obtained. Derived from (17)–(19), the average three-phase output power is given by

$$P_o = 3U_P\frac{N_1}{N_1+N_2}\frac{kI_{Lavg}}{2\sqrt{2}}I_{Lavg} \quad (20)$$

The grid-connected current is usually phase lagged caused by the output filter, however, the unity power factor and the reactive power adjustment of the grid can be realized by adjusting angle θ. Taking the Interval I as an example, ωt(0,π/3), derived as

$$u_{ab} = \sqrt{2}U_P \sin(\omega t + \theta) - \sqrt{2}U_p \sin\left(\omega t - \frac{2\pi}{3} + \theta\right)$$
$$= \sqrt{6}U_p \cos\left(\omega t + \theta - \frac{\pi}{3}\right) \qquad (21)$$

$$u_{cb} = \sqrt{2}U_P \sin\left(\omega t + \theta + \frac{2\pi}{3}\right)$$
$$- \sqrt{2}U_p \sin\left(\omega t + \theta - \frac{2\pi}{3}\right)$$
$$= \sqrt{6}U_p \cos(\omega t + \theta) \qquad (22)$$

To ensure the normal operating of the CSI, the conditions uab > UPV and ucb > UPV must be met, that is

$$\begin{cases} \sqrt{6}U_p \cos\left(\omega t + \theta - \frac{\pi}{3}\right) > U_{PV} \qquad (23) \\ \sqrt{6}U_p \cos(\omega t + \theta) \end{cases}$$

The following equation is derived from the aforementioned equation:

$$\begin{cases} -\arccos\left[\frac{U_{PV}}{\sqrt{6}U_p}\right] < \omega t + \theta - 60^0 < \arccos\left[\frac{U_{PV}}{\sqrt{6}U_p}\right] \\ -\arccos\left[\frac{U_{PV}}{\sqrt{6}U_p}\right] < \omega t + \theta < \arccos\left[\frac{U_{PV}}{\sqrt{6}U_p}\right] \end{cases} \qquad (24)$$

When UPV = 96 V and the variation range of the grid voltage is ±10%, the phase adjusting range of the grid-connected current is −18.58◦ < θ < 18.58◦.

ANALYSIS OF HF SWITCHING PROCESS

Here, Llk1, Llk2 are the leakage inductors of L1 and L2, respectively, and C_s and C_{sc} are the junction capacitors of S and Sc, respectively, which are much smaller than Cc. Sc operates in the half switching period Ts/2 when energy storage time is shorter and after S is turned OFF, and the switching frequency of Sc is half of S. There are 14 different operating intervals within one HF switching period TS , the former six operating intervals (t0–t6) can be considered as special example of the latter eight ones (t7–t14). The HF switching process waveforms and the equivalent circuits in the latter eight operating intervals (t7–t14) of the inverter is shown in Fig. 6.
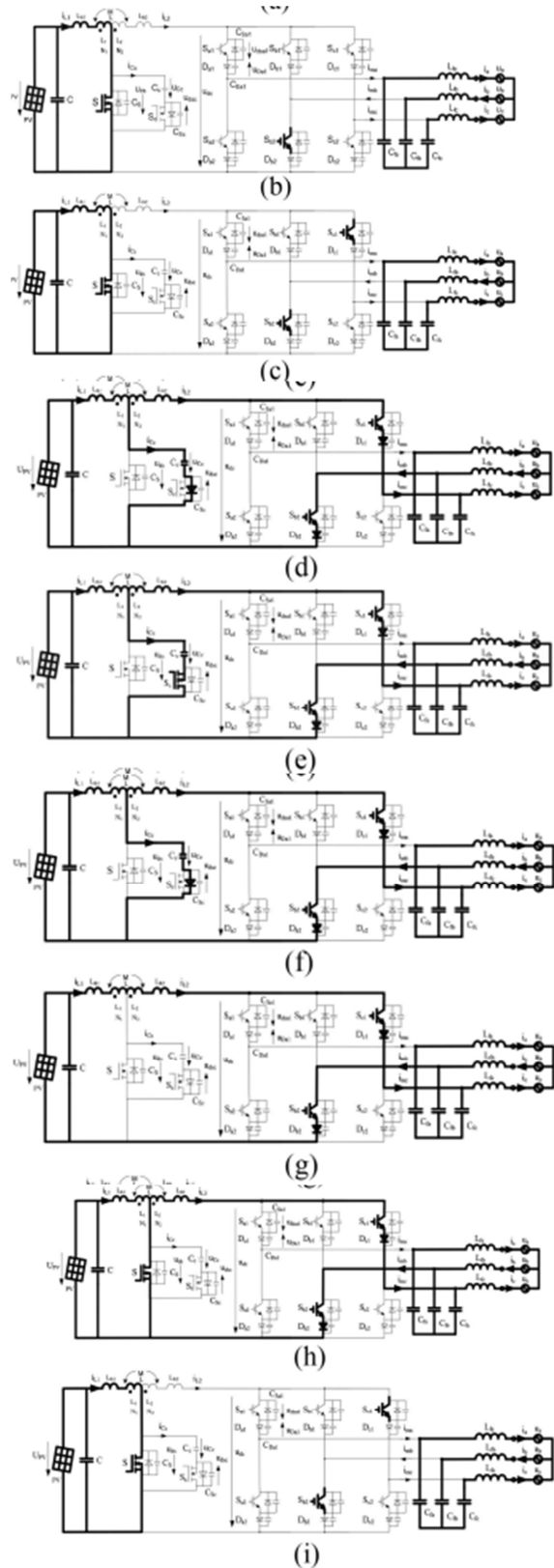

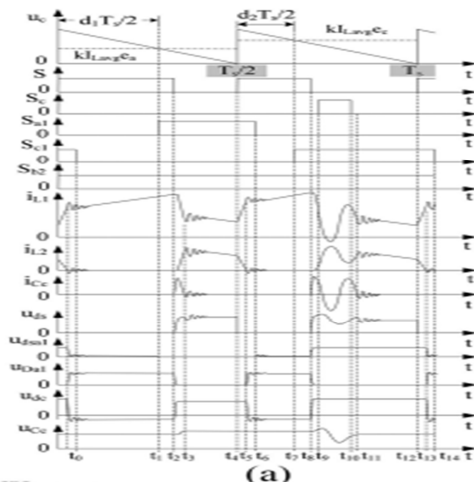(a)

(b)

(c)

(d)

(e)

(f)

(g)

(h)

(i)

Fig. 6. HF switching process waveforms and equivalent circuits in the operating intervals of the proposed inverter

1) [t6–t7]: At t6, Sa1 is turned OFF with zero current switching (ZCS). In this interval, Llk1, and Llk2 resonate with the equivalent junction capacitor of a bridge arm and iL1, iL2, and udc damply oscillate. L1 charges energy via the path of UPV , L1, and S, and ia, ib, and ic are maintained by Cf a, Cf b, and Cf c, respectively.

2) [t7–t8]: At t7, Sc1 is turned ON; S is still ON to ensure the energy is reliably released in L. The operating state of the inverter is similar to interval t6–t7.

3) [t8–t9]: At t8, S is turned OFF, uds rapidly increases to uCc and udsc rapidly decreases to zero by the energy of L1, then the parasitic diode of Sc is conducted and uds is clamped at uCc. Cc resonates with Llk1 and Llk2, the sub circuit current of energy storage switch decreases, iL2 increases from zero until meeting the equation (N1 + N2)iL2(t9) = N1iL1(t8) at t9. UPV and L1 deliver power to the grid via the path of L2, Sc1, Dc1, Lf c, uc, ub, Lf b, Sb2, and Db2, ia is maintained by Cf a.

4) [t9–t10]: At t9, Sc is turned ON with zero voltage switching. Cc continues to resonate with Llk1 and Llk2, the operating state of this interval is similar to interval t8–t9.

5) [t10–t11]: At t10, iCc > 0 and Sc is turned OFF, iCc flows through the parasitic diode of Sc, the operating state of this interval is similar to interval t9–t10.

6) [t11–t12]: At t11, iCc decreases to zero, then Llk1 and Llk2 resonate with Cs, Cc, and Csc, UPV and L deliver power to the grid via the path of Sc1, Dc1, Lf c, Lf b, Sb2, and Db2, ia is maintained by Cf a.

7) [t12–t13]: At t12, S is turned ON, then Llk1 and Llk2 make iL1 increasing gradually and iL2 decreasing gradually until iL1 and iL2 meet the equation N1iL1(t13) = (N1 + N2)iL2(t12) at t13, UPV and L deliver power to the grid via the path of Sc1, Dc1, Lf c, Lf b, Sb2, and Db2, ia is maintained by Cf a.

8) [t13–t14]: At t13, iL2 decreases to zero, Llk1 and Llk2 resonate with the equivalent junction capacitor of a bridge arm, iL1, iL2, and udc damply oscillate. In this interval, L1 charges energy via the path of UPV, L1, and S, ia, ib, and ic are maintained by Cf a, Cf b, Cfc, respectively.

DESIGNING CRITERION OF CENTER-TAPPED ENERGY STORAGE INDUCTOR

Taking the first 60° interval as shown in Fig. 2(a) as an example, the duty ratio of the energy storage switch S in a switching period Ts is given by

$$d = d_1 + d_2 = 1 - \frac{kI_{Lavg}(e_a+e_c)}{2} = 1 - kI_{Lavg}|e_b|/2 \qquad (25)$$

Substituting (15) into the aforementioned equation, gives

$$d = 1 - \frac{(N_1+N_2)U_{PV}|e_b|}{N_2|e_b|U_{PV}+3\sqrt{2}N_1U_P\cos\theta/2} \qquad (26)$$

Substituting cos θ = 1, the minimum of |eb| is √3/2, and d ≤ 0.7 into (26), the turns ratio is N2/N1 ≥ 1.75, where N2/N1 = 2 is chosen. The following equation is derived from (15):

$$K = kI_{Lavg} = \frac{2(N_1+N_2)U_{PV}}{N_2U_{PV}+3\sqrt{2}/2N_11.1U_P} \qquad (27)$$

the peak value of the grid-connected phase current can be de rived from (18)–(20) as

$$\sqrt{2}I_P = \frac{N_1}{N_1+N_2}\frac{KI_{Lavgmax}}{2} = \sqrt{2}\frac{P_o}{3U_P} \qquad (28)$$

Where ILavgmax is the ILavg corresponded to the peak value of the grid-connected phase current. The input current ripple under full load is 15%, then

$$\frac{\Delta i_L}{i_L} = \frac{1}{I_{Lavgmax}}\frac{U_{PV}}{L_1}d_{max}T_S \leq 15\% \qquad (29)$$

L1 ≥ 0.068 mH, L1 is chosen 0.068 mH, and L = 0.612 mH. The high flux iron silicon core of PHD60 is selected, where the effective length of magnetic circuit le = 34 cm, with core crosssectional area S = 4 cm2.

FUZZY CONTROL SYSTEM

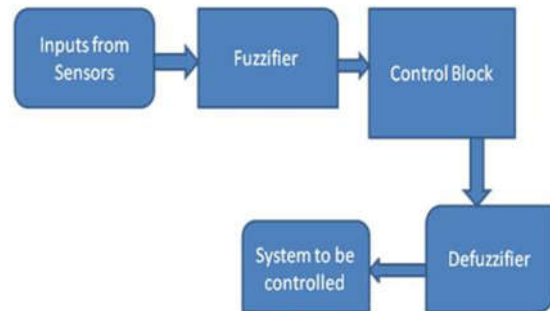A fuzzy control system consists of the following components:

Fig 7 Fuzzy Logic Controller

Control Block
A Controller which performs the fuzzy logic operation of assigning the outputs based on the linguistic information. It performs approximate reasoning based on human way of interpretation to achieve the control logic. The controller consists of the knowledge base and the inference engine. The knowledge base consists of the membership functions and the fuzzy rules, which are obtained by knowledge of the system operation according to the environment.

Defuzzifier
The Defuzzifier converts this fuzzy output to the required output to control the system.

SIMULATION RESULTS

The open circuit voltage of PV control test system is set at 112.4 V, the short circuit current 37.05 A, the MPPT PSO voltage 96.2 V, the current 34.75 A, and the Fuzzy control 3430 W. Keeping in mind the end goal to acquire exchanging cover, the important power turns are killed with delay by dead-band generator in the DSP. The planned model test consequences of 3-kW single-arrange three-stage current-source PV network associated inverter with high VTR under the setting condition are appeared in Fig. 8.
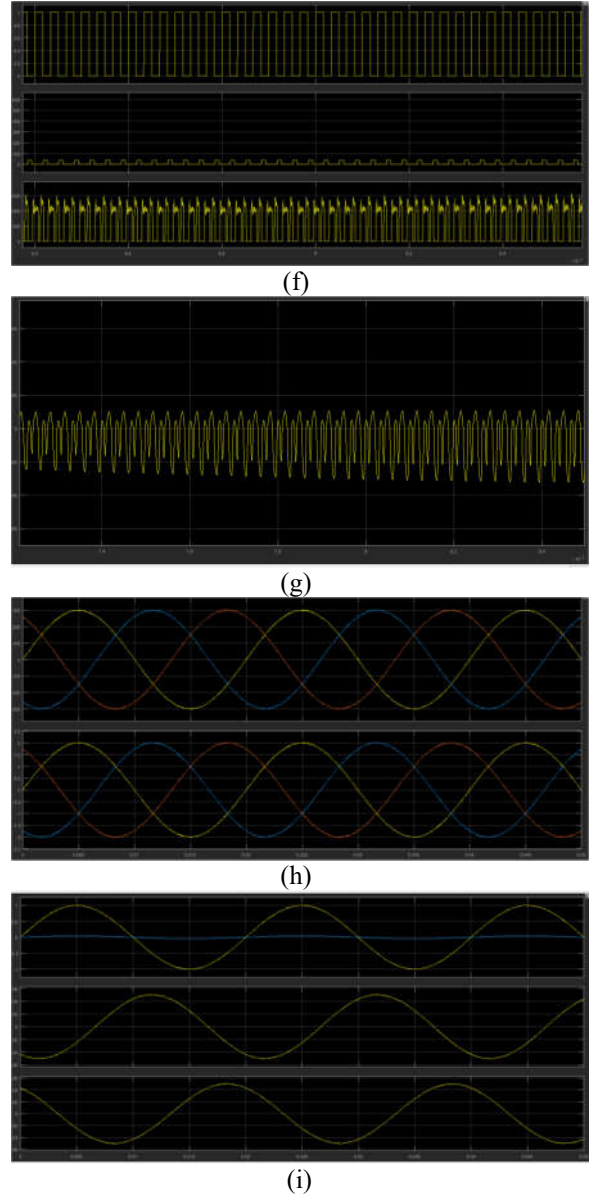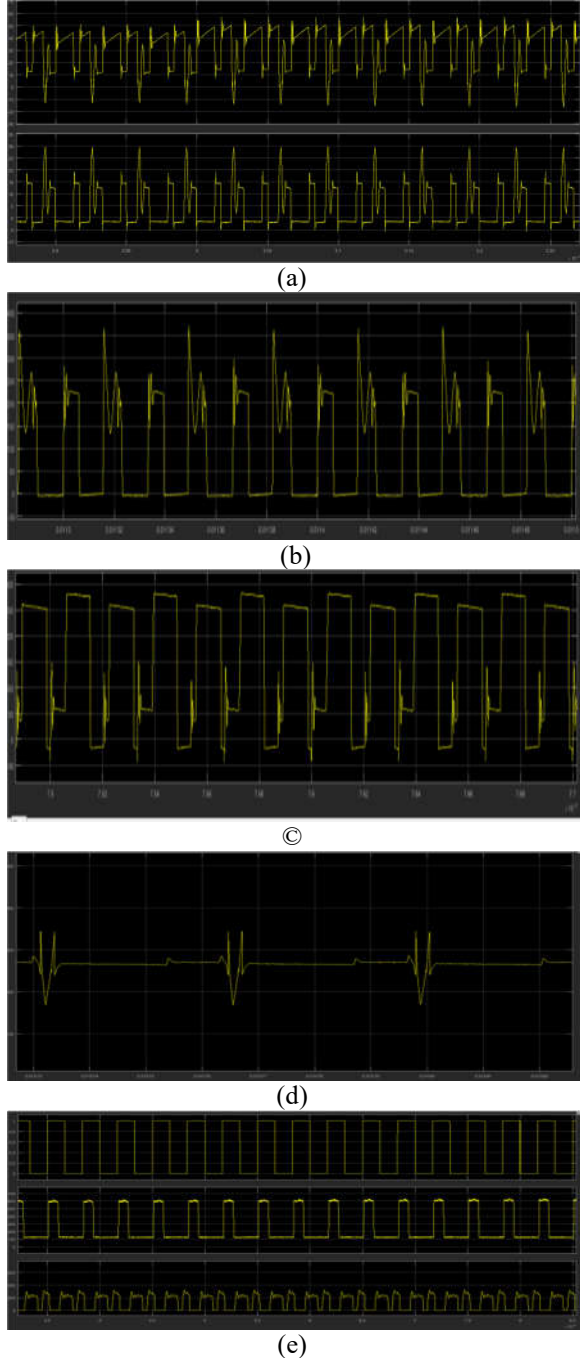
(a)

(b)

©

(d)

(e)

(f)

(g)

(h)

(i)

Fig. 8(a). Simulation waveforms of inverter under setting MPPT fuzzy condition. (a) iL1, iL2. (b) Drive signal ugs and drain-source voltage uds of S. (c) Drive signal ugsc and drain–source voltage udsc of Sc. (d) Clamping capacitance voltage uCc. (e) HF expanded of udsa1, ugsa1, and uDa1 in Interval I. (f) HF expanded of udsa2, ugsa2, and uDa2 in Interval IV (g) DC side voltage udc of bridge arm.(h) Output filter capacitance voltage uCfa, uCfb, uCfc. (i) Three-phase grid-connected current ia , ib , ic and Phase-a grid voltage ua .

The trial results have demonstrated that:

     1) The waveforms of energy storage inductor current iL1 and iL2 and their HF extended

waveforms are appeared in Fig. 8(a) and (b), which show Llk1 and Llk2 resonate with Cs and Csc or the proportional intersection capacitor of bridge arm;

2) the drive flag ugs and drain– source voltage uds of S and their HF extended waveforms are appeared in Fig. 8(c) and (d), which show the envelope of uds is the superposition of dc segment and the relating yield line voltage wave;

3) the drive flag ugsc and the drain– source voltage udsc of Sc and their HF extended waveforms are appeared in Fig. 8(e) and (f), which demonstrate that its exchanging frequency is half of S, and the swaying is caused by the reverberation between Llk1, Llk2, and Cc;

4) the bracing capacitor voltage uCc and its HF extended waveforms are appeared in Fig. 8(g) and (h), which demonstrate uCc withstands the drain– source voltage spikes of S;

5) the dc voltage udc of bridge arm and its HF extended waveforms are appeared in Fig. 8(i) and (j), which indicate the envelope of udc contrasts to its relating line voltage;

6) the drive flag, the drain–source voltage of vitality discharge switches, and the voltage of blocking diodes in the bridge arm alongside their HF extended waveforms in various interims are appeared in Fig. 8(k)– (r), which show the waveforms of upper and lower connect arm are not totally symmetrical;

7) the voltage of output filter capacitor are appeared in Fig. 8(s), which demonstrates a decent symmetry of three-stage filter voltage;

8) the waveforms of three-stage network associated current and stage a grid voltage are appeared in Fig. 8(t), which indicate the three-stage network associated current waveforms have a high caliber and are in period of matrix voltage, with a present aggregate consonant mutilation (THD) 2.68%;

9) the dynamic following MPPT waveforms under start-up and light power change are appeared in Fig. 7(u), which show the framework accomplishes its MPP after 3 s with quick MPPT following rate, high dependability, and smooth PV yield current iPV, in the interim the matrix associated current ia can rapidly be followed in the unexpected procedure of light power from 1000 W/m2 → 500 W/m2 → 700 W/m2

The change effectiveness bends of furthered three-stage PV grid-connected associated inverter under three diverse MPP volt periods of PV cells 86, 96, and 103 V is appeared in Fig. 9. The effectiveness under evaluated powersystem associated intensity of 3 kW is, respectively, 92.29%, 93.48%, and 94.06%, with a most extreme productivity, separately, 94.25%, 94.50%, and 94.75% around 1500 W. Particularly, the change effectiveness is up to 95.34%

when UMPP = 110 V. The primary loss of inverter incorporates control switch and blocking diodes misfortunes and the iron misfortune, copper loss of vitality stockpiling inductor. The characteristic misfortune commands under less network associated influence, however the conduction loss of influence switches and blocking diodes and the copper loss of vitality stockpiling inductor overwhelms under bigger matrix associated influence.
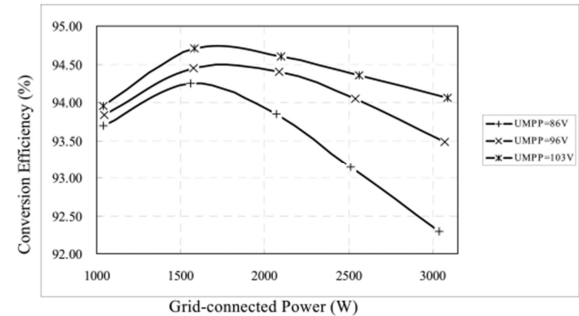

Fig. 9. Conversion efficiency curves of furthered inverter.

CONCLUSION

The proposed two-loop improved zone SPWM control strategy can ensure the normal operation of the CSI in any HF switching period with the condition that output line voltage are not smaller than input voltage, i.e., $\sqrt{6}/2Up \geq UPV$, and the reactive power adjustment of the system is realized. The proposed topology inverter is a sequentially cascaded of the input filter capacitor, the center tapped energy storage inductor, three-phase inverting bridge with six serial blocking diodes, and output CL filter, with an energy storage switch connected between the center tap of L and the negative end of the input source. The simulation results are obtained by using Matlab software and the output waveforms are shown. There are six operating intervals in one output line frequency period, each operating interval has three operating modes; the active clamped sub circuit can effectively suppress the turn-off voltage spike of S caused by the leakage inductor, and there are 14 different operating intervals within one HF switching period Ts. The design criterion of the center-tapped energy storage inductor is derived.

REFERENCES

1] T. K. S. Freddy, N. A. Rahim, W. P. Hew, and H. S. Che, "Modulation techniques to reduce leakage current in three-phase transformerless H7 photovoltaic inverter," IEEE Trans. Ind. Electron., vol. 62, no. 1, pp. 322– 331, Jan. 2015.

[2] T. Messo, J. Jokipii, J. Puukko, and T. Suntio, "Determining the value of DC-link capacitor to ensure stable operation of a three-phase photo voltaic inverter," IEEE Trans. Power Electron., vol. 29, no. 2, pp. 665–673, Feb. 2014.

[3] J. Ji et al., "A simple differential mode EMI Suppressor for the LLCL filter-based single-phase grid-tied transformerless inverter," IEEE Trans. Ind. Electron., vol. 62, no. 7, pp. 4141–4147, Jul. 2015.

4] I. Serban, "Power decoupling method for single-phase H-bridge inverters with no additional power electronics," IEEE Trans. Ind. Electron., vol. 62, no. 8, pp. 4805–4813, Aug. 2015. [5] B. Singh, C. Jain, and S. Goel, "ILST control algorithm of single-stage dual purpose grid connected solar PV system," IEEE Trans. Power Electron., vol. 29, no. 10, pp. 5347–5357, Oct. 2014.

[6] D. Barater, G. Buticchi, E. Lorenzani, and C. Concari, "Active common mode filter for ground leakage current reduction in grid-connected PV converters operating with arbitrary power factor," IEEE Trans. Ind. Electron., vol. 61, no. 8, pp. 3940–3950, Aug. 2014.

[7] L. S. Garcia et al., "Modeling and control of a single-stage current source inverter with amplified sinusoidal output voltage," in Proc. IEEE Appl. Power Electron. Conf., 2012, pp. 2024–2031.

[8] R. T. H. Li, H. S. H. Chung, and T. K. M. Chan, "An active modulation technique for single-phase grid-connected CSI," IEEE Trans. Power Electron., vol. 22, no. 4, pp. 1373–1382, Jul. 2007.

[9] D. Chen, Y. Qiu, Y. Chen, and Y. He, "Nonlinear PWM-controlled single phase boost mode grid-connected photovoltaic inverter with limited storage inductance current," IEEE Trans. Power Electron., vol. 32, no. 4, pp. 2717–2727, Apr. 2017

[10] B. N. Alajmi, K. H. Ahmed, G. P. Adam, and B.